Scientific Research Publishing

Open Journal of Civil Engineering, 2025, 15(4), 832-849
https://www.scirp.org/journal/ojce
ISSN Online: 2164-3172
ISSN Print: 2164-3164

Butterfly Wing Microstructures for Bioinspired Thermal Insulation in Energy-Efficient Buildings in West Africa

Guomin Liu[1*], Seydou Diarrassouba[2*], Chancellor Clever Kudakwashe Jijita[2], Haoqing Chen[1], Yongxu Chen[1], Yao Chen[1]

[1]School of Civil Engineering, Jilin Jianzhu University, Changchun, China
[2]International Exchange College, Jilin Jianzhu University, Changchun, China
Email: *lgm951@163.com, *diarrassoubaseydou590@gmail.com

How to cite this paper: Liu, G.M., Diarrassouba, S., Chancellor, C.K.J., Chen, H.Q., Chen Y.X. and Chen, Y. (2025) Butterfly Wing Microstructures for Bioinspired Thermal Insulation in Energy-Efficient Buildings in West Africa. *Open Journal of Civil Engineering*, **15**, 832-849.
https://doi.org/10.4236/ojce.2025.154047

Received: October 2, 2025
Accepted: December 19, 2025
Published: December 22, 2025

Abstract

This study explores the potential of butterfly wing microstructures as inspiration for thermal insulation solutions in buildings located in hot and humid climates, such as those of West Africa. The morphological features of *Papilio maackii*, *Papilio xuthus*, and *Kaniska canace* were analyzed using scanning electron microscopy, modeled in AutoCAD, and simulated in COMSOL Multiphysics under realistic climatic boundary conditions. Thermal performance was assessed through surface temperature, heat flux, and radiosity. Among the tested designs, the *Papilio xuthus*-inspired panel exhibited the best performance, with the lowest peak surface temperature, reduced average heat flux, and minimized radiosity. In contrast, conventional wall panels demonstrated the highest thermal losses, while *Papilio maackii* and *Kaniska canace*-based designs showed intermediate performance. These findings demonstrate the potential of butterfly wing-inspired geometries to significantly improve thermal resistance and contribute to energy-efficient building design in tropical regions.

Keywords

Butterfly Wing Microstructures, Bionic Engineering, Thermal Insulation, COMSOL Simulation, Energy-Efficient Buildings, West Africa

1. Introduction

With rapid urbanisation across West Africa, traditional insulation systems are increasingly unable to manage the thermal loads and energy demands generated by persistent heat and humidity. Recent studies highlight that conventional insula-

tion materials cannot adequately meet global energy-efficiency requirements, reinforcing the urgent need for alternative strategies [1] [2]. In hot and humid climates, these limitations result in excessive reliance on active cooling systems, higher energy consumption, and reduced indoor comfort, making energy-efficient building design a pressing challenge for the built environment [3] [4]. Reports further indicate that traditional building construction in the region rarely achieves thermal comfort under current climatic conditions, underlining the urgency of developing climate-adapted insulation solutions [5] [6].

Biomimicry, the design and manufacturing of systems inspired by biological structures and functions, offers a promising pathway for passive thermal regulation in architecture [7]. Among natural thermoregulators, butterfly wings stand out for their remarkable ability to manage heat and light efficiently through hierarchical micro- and nanostructures. Overlapping scales form reflective surfaces and air pockets that impede heat transfer, enhancing insulation and thermal control [8]. These properties are structural rather than pigment-based, with features such as high solar reflectivity, anisotropic light scattering, and low thermal conductivity making butterfly wings highly relevant for passive cooling applications. Their capability to trap air, restrict thermal conduction, and reflect solar radiation provides a natural model for improving building insulation materials [9] [10].

This study investigates the potential of butterfly wing-inspired microstructures to enhance the thermal insulation of wall panels tailored to the hot and humid climatic conditions of West Africa. By integrating biological morphology with engineering simulations, the research aims to contribute to energy-efficient building design and improved indoor thermal comfort in tropical regions.

2. Overall Morphological Analysis of Butterfly Wing Surface

2.1. Morphological Analysis of *Papilio maackii*

As illustrated in **Figure 1(a)**, low-magnification microscopy (5×) reveals that the forewing of the butterfly exhibits a triangular outline bordered by evenly distributed black cilia. The distance between the wing root and its distal margin is about 3 cm, longitudinal veins run outwards and divide the surface into irregular polygonal areas. The wing scales are mostly green with some black lines stretching across and the ones near the margins show bright green iridescence when exposed to light. **Figure 1(b)** demonstrates that the wing surface consists of two different layers of scales: a basal layer of scales that is black and an overlaying layer of scales, where neighboring scales overlap to some extent, resulting in bright coloration under exposure to light. On greater magnification, the scales are long and narrow with a length of up to 150 μm and a maximum width of 50 μm. The upper edges of many of these scales are serrated, but the bright-coloured scales have smooth edges, and look like narrow willow-leaves (**Figure 1(c)**). Each scale has one colour, and in any case, matte yellow or iridescent green. The orderly, tile-like arrangement across the wing generates the characteristic vibrant pattern [11].

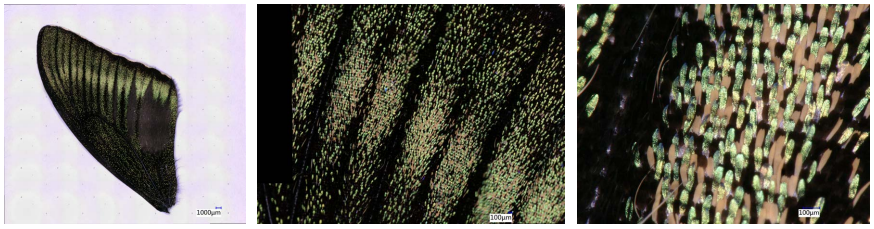

(a) (b) (c)

Figure 1. *Papilio maackii* front wing [11]. (a) 5:1, (b) 15:1, (c) 150:1.

2.2. Morphological Analysis of *Papilio xuthus*

As shown in **Figure 2(a)**, Ultra-Depth Three-Dimensional Microscopy reveals that the forewing of *Papilio xuthus* exhibits a triangular profile, measuring approximately 4.6 cm in maximum length and 2.75 cm in maximum width. It has a wing design that consists of black and white stripes in rotation along the wing root, to the margins. These stripes run along the wing veins in the central area with a series of curved and crescent-shaped spots forming outer edges where they have no iridescence or pigment reflections. As it is observed in the marginal scales, in more detail (**Figure 2(b)**), the black and the white scales are regularly arranged, with white scales forming triangular patches surrounded by black scales, developing a more specific alternating scheme. An increase in magnification of the black-white boundary (**Figure 2(c)**) reveals a sharply defined distribution, with both black and white scales exhibiting similar morphology, approximately 150 μm in longitudinal length and 60 μm in lateral width [11].

(a) (b) (c)

Figure 2. *Papilio xuthus* wing [11]. (a) 5:1, (b) 15:1, (c) 50:1.

2.3. Morphological Analysis of *Kaniska canace*

As shown in **Figure 3(a)**, the forewing of *Kaniska canace* measures approximately 2.6 cm in length and 0.7 cm in width, displaying an irregular, triangular outline with pronounced undulations. The wing exhibits a black background that darkens progressively from the root toward the margin, with the apex marked by prominent white bands resembling tree-bark patterns. Magnified observation of the black–white boundary region (**Figure 3(c)**) reveals interspersed scales of both colors. Under 150× magnification (**Figure 3(b)** and **Figure 3(d)**), both white and black scales measure approximately 150 μm in length and 50 μm in maximum width, each bearing three serrations along the upper posterior edge. The morphology of the scales is therefore nearly identical, differing only in pigmentation [11].

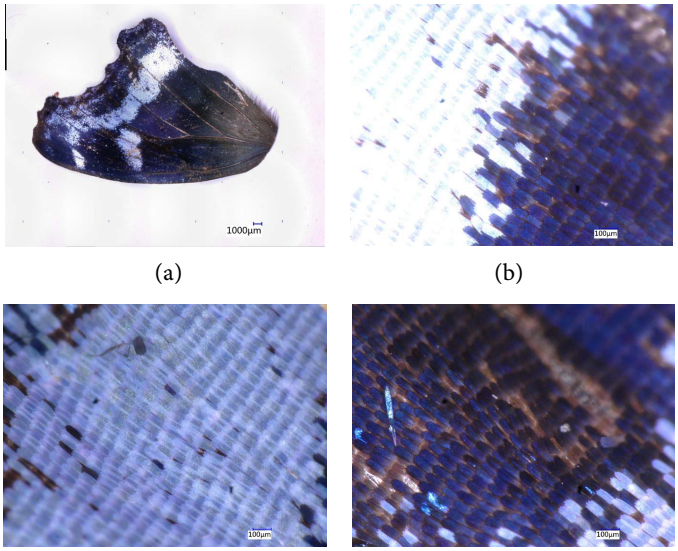

(a) (b)

(c) (d)

Figure 3. *Kaniska canace* wing [11]. (a) 5:1, (b) 150:1, (c) 150:1, (d) 150:1.

3. Microscopic Morphology and Structural Analysis of Butterfly Wing Scales

3.1. *Papilio maackii*

Scanning electron microscope (SEM) image of **Figure 4(b)**, butterfly wing scale surface at magnification 500x. The microstructure has a set of parallel ridges arranged in a highly ordered way, as shown in **Figure 4(b)**, the structure resembles willow leaves. Further magnification at 5000x reveals branching along both sides of the ridge, as illustrated in **Figure 4(a)**. **Figure 4(c)** provides additional morphological details, showing that the surface in between the ridges is occupied by a network-like mesh structure, consisting of hexagonal or irregular polygonal cavities. These vein-like micro structures are light-trapping pits and microcavities and boost scattering, reflection, and absorption of incident light. Morphology indicates a lamellar structure, the ridges are used to achieve the structural stability and create optical pathways, and the porous mesh enables the amplified photothermal conversion and structural coloration. Geometrically, the inter-ridge (vein) distance has a value of about 3 μm and the average pit sizes have dimensions of about 0.6 μm in length and 0.3 μm in width [11].

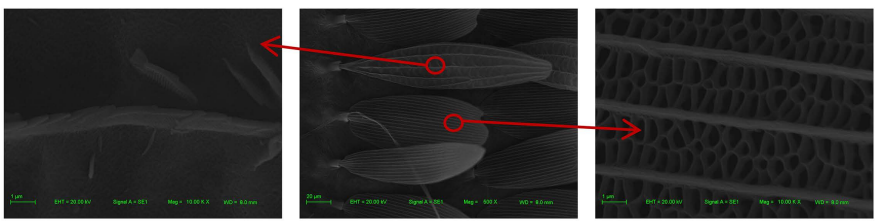

(a) (b) (c)

Figure 4. Scanning image of the *Papilio maackii* wing [11]. (a) 5000:1, (b) 500:1, (c) 10,000:1.

3.2. *Papilio xuthus*

Scanning electron microscope (SEM) image of the butterfly wing scale surface at 500x magnification is shown in Figure 5(a). Each scale exhibits a similar shape, as can be observed in Figure 5(a). Further morphological details are presented in Figure 5(b), where the surface reveals are a series of parallel ridges oriented horizontally, forming the primary structural framework of the scale. Between these ridges lies a network of irregularly structural microcavities, most of which are circular or elliptical pits. Notably, the image shows both nearly circular pits and elongated elliptical pits, illustrating the diversity of cavity morphology within the mesh-like structure. The circular pits exhibit isotropic geometry, whereas the elliptical pits display pronounced anisotropy with distinct long and short axes. Quantitative analysis indicates that the average distance between adjacent ridges is approximately 2.6 μm, while the pits have an average length of 0.8 μm and width of 0.3 μm [11].

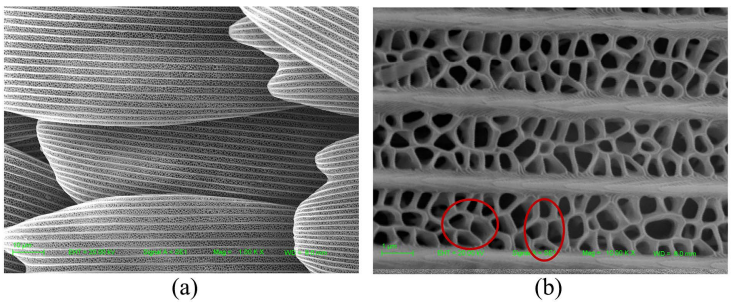

(a) (b)

Figure 5. Scanning images of the *Papilio xuthus* wing [11]. (a) 500:1, (b) 10,000:1.

3.3. *Kaniska canace*

Figure 6(a) shows a scanning electron miscroscope (SEM) image of a butterfly wing scale at 500x magnification, highlighting the orderly arrangement of the scales. Each scale exhibits approximately 7 to 8 serrations at the top. In Figure 6(b), the surface is characterized by parallel ridges running diagonally, forming the primary structural framework. Periodically placed elliptical pores or cavities are located between these ridges. Although the pore sizes vary slightly, they are uniformly distributed within the ridge structure. Morphometric analysis indicates that the mean distance between adjacent ridges is approximately 1.2 μm, and the elliptical pits have average dimensions of 0.8 μm in length and 0.3 μm in width [11].

In conclusion, based on the size and parameter values of the SEM images of the three butterfly wings the shape and morphology of the units as well as the structural distribution were compiled and listed in Table 1.

Following the morphological analysis, the extracted microstructural parameters of the butterfly wings summarize in Table 1 were used as the basis for constructing a 3D CAD model of a bioinspired thermal insulation panel. These characteristic dimensions were scaled up to functional sizes suitable for wall panel integration, while preserving the geometric integrity of the original biological features.

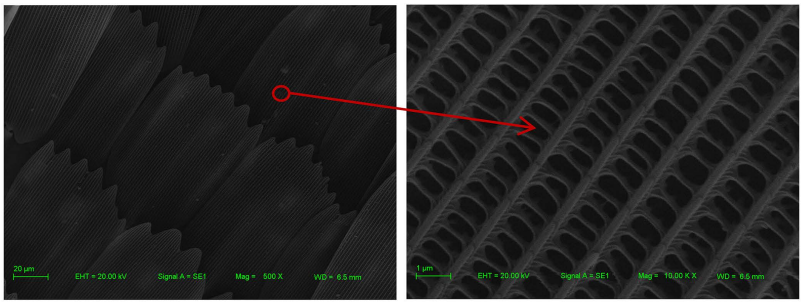

(a) (b)

Figure 6. Scanning images of the *Kaniska canace* wing [11]. (a) 500:1, (b) 10,000:1.

Table 1. Analyze the table of characteristic parameters of butterfly microstructure.

Types of scales	Distance between veins	Length of pit	Width of pit
Papilio maackii front wing	3 μm	0.6 μm	0.3 μm
Papilio xuthus	2.6 μm	0.8 μm	0.3 μm
Kaniska canace	1.2 μm	0.8 μm	0.3 μm

We will scale up the sizes of the butterfly's wing microstructures to 10, in order to convert every unit to millimeters without losing important dimensionless parameters of aspect ratio, periodicity and surface-to-volume ratio. Scaling laws of heat transfer and wave propagation [12] show that scaling geometry at constant material refractive index and ratio of thermal conductivity ratios holds the dimensionless, Nusselt, Biot, and optical interference numbers fixed, and leaves the functional behavior of the system the same. This means that the 10 mm scale model scales down microscale light scattering, multi reflection and confinement of localized heat, which effectively scales the photothermal regulation mechanisms shown by the butterfly to a scaleable macro scale such that can be analyzed in the context of architectural insulation [12] [13].

The scaling was performed using the magnification equation [14] (I):

$$M = I/A \tag{I}$$

$$I = M \times A \tag{II}$$

$$I = 1\times10^{-6} \times 10000$$

$$I = 0.01\,\text{m} = 10\,\text{mm}$$

where:

M is the magnification factor, I is the target (scaled) dimension used in the wall panel, A is the actual size of the biological microstructure. After scaling up every value in **Table 1**, we will use those values to construct the 3D model of each model using AutoCAD, which can be observed in **Figure 7**.

3.4. Simulation Setup and Parameters

3.4.1. Parameters and Material Selection

The exterior convective heat transfer coefficient for sun-exposed vertical façades was taken as 12 - 15 $W \cdot m^{-2} \cdot K^{-1}$. This range corresponds to the combined natural +

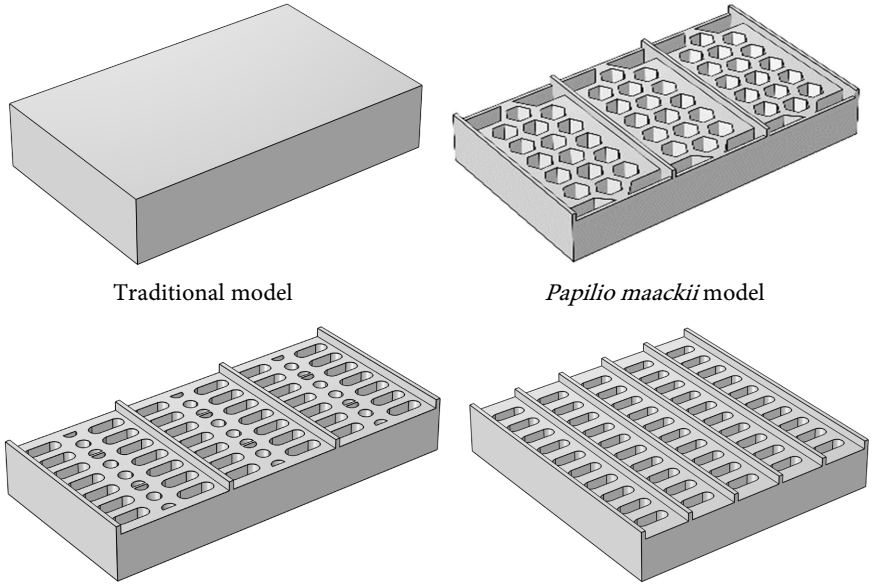

Figure 7. The model of the butterfly's scale wing.

forced convection model commonly used in building simulation h = 5.7 + 3.8 Vz (McAdams's form implemented in EnergyPlus), where Vz is the local wind speed. The chosen range (≈1.7 $m \cdot s^{-1}$ - 2.5 $m \cdot s^{-1}$) represents light–to–moderate effective wind conditions typical of sheltered or partially sheltered urban façades in Abidjan [15]-[17]. The indoor air movement used the internal value of 5 - 7 $W/m^2 \cdot K$ in the simulation. For boundary conditions, the temperature inside the room is set 25˚C at a constant room temperature, and the outside, 28˚C representative of average climatic conditions in Abidjan Côte d'Ivoire [18].

To further analyses the thermal insulation performance, we simulated and analyzed in terms of total temperature and total surface heat flux, surface radiosity through the Fluent module in Consol multiphysics. First, the three models were given common material attributes. The model material used is polylactic acid (PLA). Although PLA is not currently used as a mainstream construction material in West Africa at the present, but its usage in the present work can be explained by its ability to be 3D printed and the possibility of being localized by using renewable biomass resources like maize and cassava [19]. An example is Cote d'Ivoire which in 2022 alone harvested an estimated 6.3 million tons of cassava, one of the leading producers of cassava in Africa and the world [20]. It is also a large-scale producer of maize and it produces about 1.1 to 1.3 million tons of maize annually which forms a large part of the cereal supply of West Africa [21]. Such rich sources of agriculture offer a long-term source of PLA which is produced locally using local starch crops like maize and cassava. Therefore, the local manufacturing plants of PLA might be established; this would allow reducing production costs dramatically and make PLA-based biomimetic insulation materials effective economically and suitable to the environment to be used in the local construction sectors. In addition, PLA also has low thermal conductivity with a range

of 0.0643 to 0.0904 W/m·K) which is significantly lower than concrete 1.0 - 1.8 W/m·K and typical clay bricks 0.82 W/m·K. Its average mass of about 1233 kg/m^3 (1.233 g/cm^3) is lightweight and efficient insulation [22]. Secondly, we set up all boundary in the software such: exterior convective heat transfer coefficient, ambient temperature, extermal radiation source generate accordingly to the coordinate (Latitude: 5.28˚N, Longitude: 4.03˚W [23]) and a normal mesh element configuration was employed in COMSOL Multiphysics to discretize the geometric domain. The mesh was generated automatically by the software, ensuring an optimal balance between computational efficiency and numerical accuracy. To be sure the mesh generated we will not affect the result we will do the mesh-independence test to confirm that numerical results are insensitive to discretisation.

3.4.2. Mesh Generation and Quality Assessment

We used COMSOL Multiphysics to set up a normal mesh and discretize the computational domains of all the four models. The automatic tetrahedral meshing algorithm was chosen because it offers a good balance between the numerical and computational efficiency. **Table 2** summarizes the mesh statistics and size parameters for each configuration.

Table 2. Mesh statistics and element size parameters for all models.

Model	Total Elements	Avg. Element Quality	Min. Element Quality	Element Volume Ratio	Mesh Volume (m^3)	Max. Element Size (m)	Min. Element Size (m)
Papilio maackii	16,210	0.6105	0.1454	0.00224	3.12×10^{-5}	0.0088	0.00158
Papilio xuthus	46,158	0.6367	0.1680	0.00408	2.31×10^{-5}	0.0079	0.00142
Kaniska canace	68,038	0.6445	0.1885	0.00502	3.26×10^{-5}	0.00646	0.00116
Traditional Model	2105	0.6734	0.2609	0.09042	2.51×10^{-5}	0.0058	0.00104

The quality of all generated meshes fell within the range of 0.61 to 0.67 average element quality that is fine in terms of steady state thermal simulations. Even though minimum element quality values slightly varied due to complex geometrical curvatures, no invalid or inverted elements were detected during automatic validation in COMSOL Multiphysics. All configurations converged successfully by the solver, and this is a good indication of numerical soundness. All the meshes used the same refinement parameters, which were: curvature factor = 0.6, narrow region resolution = 0.5 and the maximum rate of element growth = 1.5 to provide smooth elements transitions at the fineness and coarse zones, without affecting the fidelity of the biomimetic microstructures. Overall, the developed meshing approach ensured a uniform geometric resolution between all the biomimetic and traditional models, allowing them to be directly compared to each other in terms

of their thermal behaviour at the same level of computation.

3.4.3. Mesh-Independence Verification

A mesh-independence test was done to ensure that mesh density did not affect numerical results. Surface averaged values of temperature, normal heat flux and surface radiosity were measured on both the Normal and Fine mesh models with the same set of boundary conditions and material properties. The test result was summarized in Table 3.

Table 3. Mesh-independence results (surface-averaged quantities).

Model	Quantity	Fine	Normal	Error (%)	Mesh-independent? (≤3%)
Papilio maackii	Temperature (˚C)	21.151	21.141	0.05	Yes
	Heat flux (W·m^{-2})	482.58	491.76	1.90	Yes
	Surface radiosity (W·m^{-2})	440.81	441.31	0.11	Yes
Papilio xuthus	Temperature (˚C)	21.073	21.080	0.03	Yes
	Heat flux (W·m^{-2})	546.46	551.27	0.88	Yes
	Surface radiosity (W·m^{-2})	439.15	439.17	0.01	Yes
Kaniska canace	Temperature (˚C)	21.219	21.231	0.06	Yes
	Heat flux (W·m^{-2})	635.54	630.33	0.82	Yes
	Surface radiosity (W·m^{-2})	442.07	442.20	0.03	Yes
Traditional	Temperature (˚C)	21.790	21.798	0.04	Yes
	Heat flux (W·m^{-2})	630.77	622.20	1.36	Yes
	Surface radiosity (W·m^{-2})	454.60	454.64	0.01	Yes

The relative percentage error for each variable was computed using:

Error (%) = (Result of fine mesh − Result of normal mesh)/Result of fine mesh [24]

The results of the mesh-independence verification in Table 3 confirm that the numerical outcomes are insensitive to spatial discretization. All the critical thermal quantities had relative deviations less than 2% and the major ones had less than 1% of deviation, which met the 3% independence criterion. The amount of temperature and radiosity was almost mesh independent, and smaller deviations in the heat flux were within reasonable numerical error. This therefore led to the conclusion that the Normal mesh setup was accurate enough to be used in further simulations and also to be computationally efficient without compromising the accuracy.

4. Model Analysis of Performance of Thermal Insulation of Butterfly Scale's Structure

4.1. Temperature Analysis of Light-Trapping Structure of Butterfly Scale

The thermal conditions of the two boundaries of the material in thermal simulation are different. The hot side (yellow color) refers to the surface directly exposed to the heat source whereas the temperatures reach its maximum while the cold side (red color) is the other side opposite to the heat source and its temperature is the lowest due to the dissipation of the energy. This can be observed in **Figure 8**. To further evaluate the thermal insulation performance. We will analyse **Figure 9** which present the temperature distributions curves along the material thickness. **Figure 9** allows to compare the traditional model to the biomimetic structure using the numerical values. As can be seen in **Figure 8**, the highest temperature calculated from the simulated radiation is in the yellow color and the low temperature is the red color. The yellow color which is the hot side and the red color which is cold side. The temperature line graphs indicate that the conventional design has the highest peak of the hot side temperature (65.17˚C at $x = 0$) and the lowest of the cold side temperature (46.71˚C at $x = 0.08$), which is accompanied by a huge temperature difference 18.46˚C. High heat transfer and consequently poor insulation are represented by this sharp drop. Conversely, the biomimetic designs (*Kaniska canace*, *Papilio maackii*, and *Papilio xuthus*) have lower peak temperatures (53˚C - 58˚C) on the hot side and higher (51˚C - 54˚C) on the cold-side, leading to significantly smaller changes in temperature 1.6 to 3.9˚C. This low gradient implies much greater thermal resistance. *Papilio xuthus* (1.63˚C drop) and *Papilio maackii* (1.89˚C drop) are the most insulated followed by *Kaniska canace* (3.89˚C drop) that exhibits mid-range performance. Therefore, the line chart substantiates the fact that butterfly-inspired microstructures provide much better thermal insulation than the conventional smooth surface.

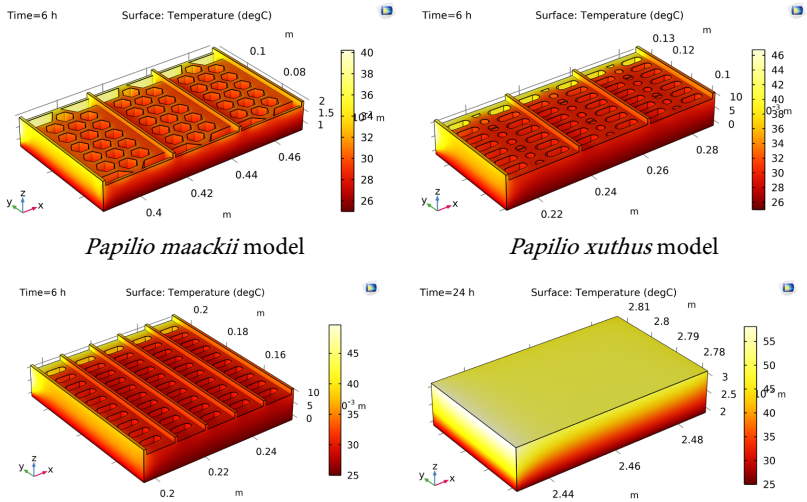

Papilio maackii model | *Papilio xuthus* model

Kaniska canace model | Traditional model

Figure 8. Temperature nephogram.

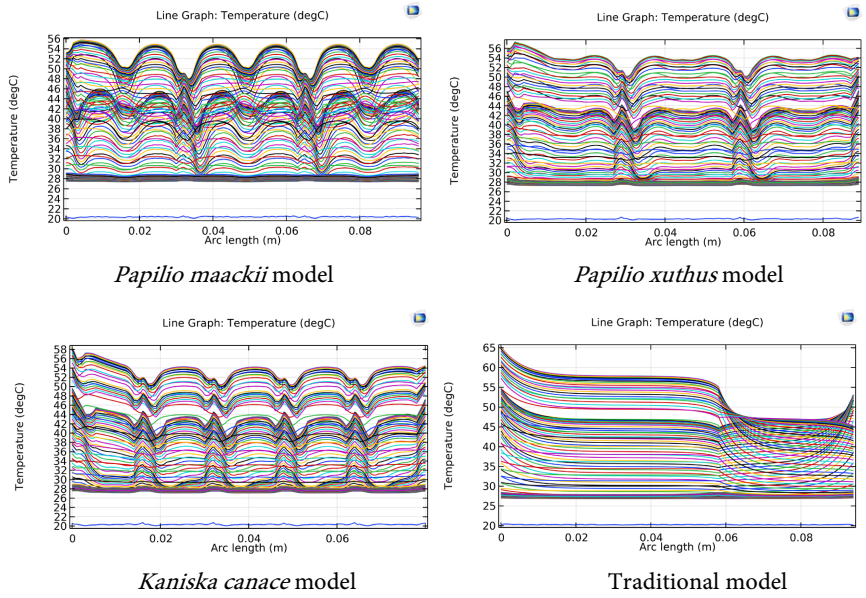

Figure 9. Temperature line chart.

4.2. Average Surface Temperature

The thermal insulation performance of models can be observed in Figure 10. The traditional structure exhibited the highest surface temperature rise, reaching a maximum of approximately 37.9˚C at 1.5 h, which corresponds to rapid heat penetration and low thermal resistance. Comparatively, the biomimetic designs based on butterfly wing designs *Papilio xuthus*, *Kaniska canace* and *Papilio maackii* had much lower heating with temperatures not exceeding 34˚C - 35˚C. This indicates a slower rate of heat transfer through the material. Moreover, the curves of the biomimetic models are flatter, with smaller temperature gradients over time, confirming their superior ability to delay and suppress heat conduction. Two of them, *Papilio xuthus* and *Papilio maackii* demonstrate the most stable profiles, which indicate the most efficient insulation. In sum, the time-temperature diagram directly supports that butterfly-inspired microstructures are better than traditional smooth surfaces to increase thermal insulation.

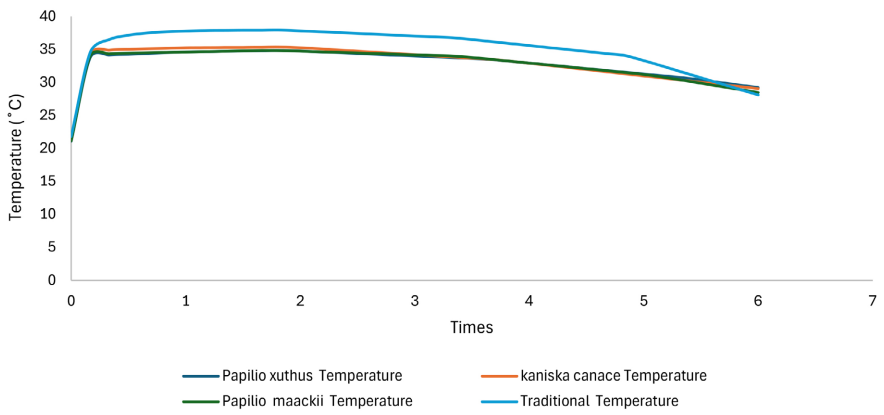

Figure 10. Temperature-time curve chart of bionic models.

4.3. Heat flux Analysis of Light-Trapping Structure of Butterfly Scale

In Figure 11, the light red shading corresponds to the hot with elevated temperature and the opposite the darker red tones are the cold side with lower temperature. To better analyses we get insight into the thermal insulation behavior in the Figure 12. Comparison of the rate and heat penetration extent can be made in these plots thus quantifying the effectiveness of every structure in thermal flow resistance. The conventional design has strong variance, with values ranging from −12.67 W/m^2 to a positive peak of 37.76 W/m^2. Such sharp bends suggest unsteady and focused heat transfer channels, which result in inefficient thermal resistance. Conversely, the butterfly-inspired systems are good at trapping and redistributing the heat. At x = 0.003 m, the surface flux of *Kaniska canace* is very high 284.71 W/m^2, but it also rapidly decreases with depth, up to a value of almost zero and even negative values −10.81 W/m^2 at x = 0.06 m. The trend of this behavior indicates intense attenuation of heat transfer because the energy is scattered and dissipated. *Papilio maackii* exhibits the same trend without the extreme initial peak. Beginning with 238.3 W/m^2 on the hot end, the flux swings in moderate −9.22 to +7.32 W/m^2 steps throughout the thickness, but with small overall magnitudes. This means that there are efficient redistribution of heat and a steady decline of thermal penetration among all designs. *Papilio xuthus* has the best stable and controlled performance of all designs. The flux in it is constantly low throughout the material, and it varies within a very narrow range of −12.82 W/m^2 to −6.40 W/m^2. The flat, suppressed curve reflects minimal and evenly distributed heat transfer, representing the most effective thermal insulation. Overall, the biomimetic microstructures reduce both the magnitude and variability of heat flux compared to the traditional surface, thereby enhancing thermal resistance.

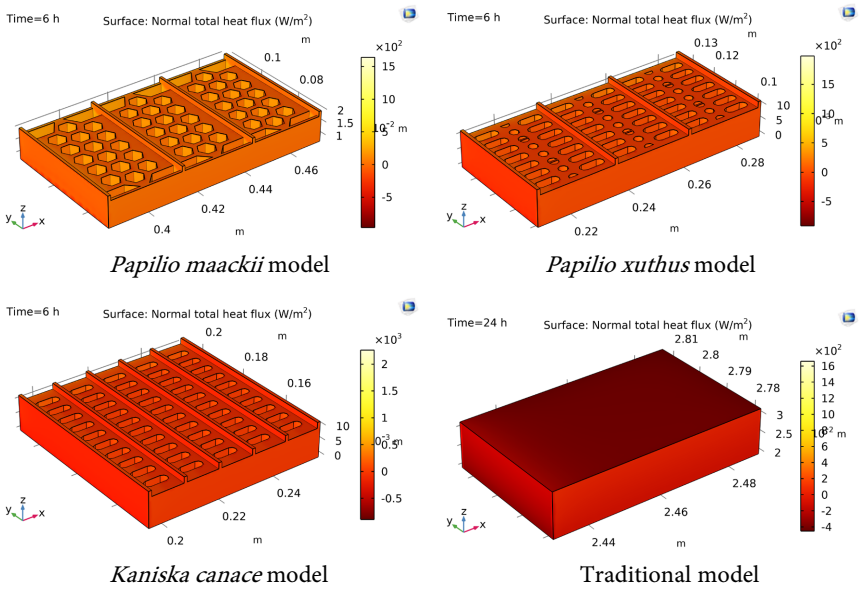

Papilio maackii model | *Papilio xuthus* model

Kaniska canace model | Traditional model

Figure 11. Heat flux nephogram.

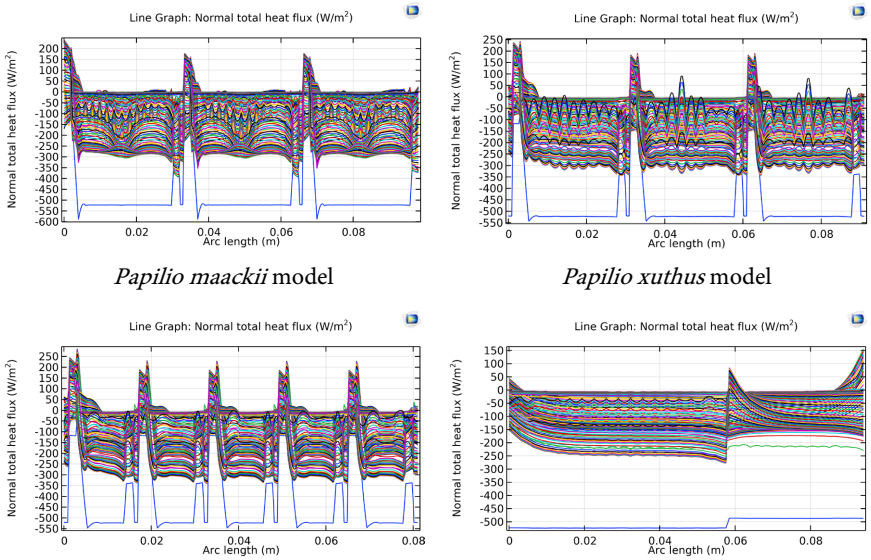

Papilio maackii model | *Papilio xuthus* model

Kaniska canace model | Traditional model

Figure 12. Heat flux line chart.

According to the curves, *Papilio xuthus* shows the best performance in insulation when compared to *Papilio maackii* and *Kaniska canace* with traditional design showing worst attitude at thermal control.

4.4. Average Surface Heat Flux

The heat flux response in **Figure 13** indicates evident differences between the traditional and bio-mimetic models. The traditional model structure demonstrates the largest initial peak 757.77 W/m^2 and the strongest negative flux that changes with time −10.44 W/m^2 at 6 h, which is in line with the fast and unstable heat transfer. The bionic models on the other hand show reduced peaks and faster suppression of flux to near zero levels, which reflects greater thermal resistance. At 584.54 W/m^2, Kaniska starts to decrease but soon levels off to −1.78 W/m^2, *Papilio maackii* and *Papilio xuthus* stabilize even at a faster rate and their flux values are very low −1.65 and −1.46 W/m^2, respectively. Of them, *Papilio xuthus* has one of the most stable and controlled behavior, which is an indicator of the best insulation. Overall, the butterfly-inspired microstructures significantly reduce both the magnitude and variability of heat flux compared to the traditional surface, hereby enhancing thermal insulation performance.

4.5. Surface Radiosity Analysis of the Light Trapping Structure of Butterfly Scales

The yellow area is the hot side corresponds to the surface direct contact with the heat source and surface radiosity is the greatest. The opposite side is the cold side which is red color has the lower temperature. This can be observed on **Figure 14**. to better compare the traditional model to the bionic, we have will observe **Figure 15** which allow to compare numerical the value of the surface radiosity of

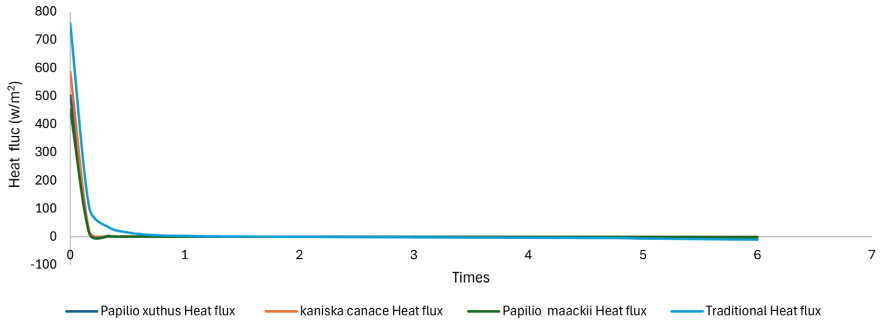

Figure 13. Heat flux-time curve chart of bionic models.

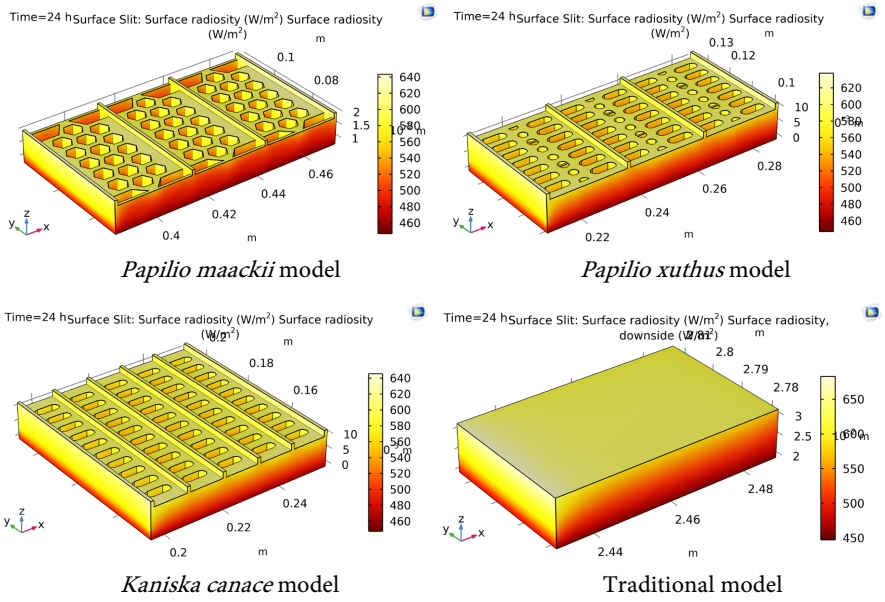

Figure 14. Surace radiosity nephogram.

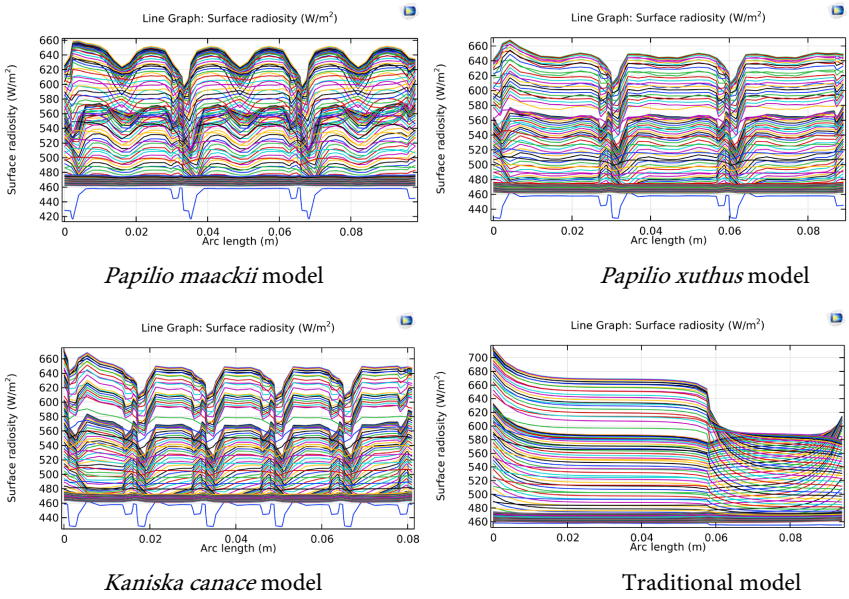

Figure 15. Surface radiosity line chart.

each model. The surface radiosity line charts clearly show the better insulation of the biomimetic models in comparison with the traditional structure. The traditional model has the greatest radiosity throughout the distance 714.82 W/m^2 to 587.90 W/m^2 at 0.08 m, with high radiative heat loss and low insulation ability. Conversely the bionic designs minimise the amount and the variation of surface radiosity. The lowest starting value is observed to be *Papilio maackii* 624.64 W/m^2 to 631.20 W/m^2 at 0.08 m and the most stable profile is *Papilio xuthus* 641.23 W/m^2 to 646.26 W/m^2 at 0.08 m with considerably less fluctuations, which implies that radiation is effectively suppressed. *Kaniska canace* 659.29 W/m^2 to 646.91 at 0.08 m demonstrates intermediate performance because the values are higher than those of the other two but overall lower than those of the traditional surface. The biomimetic models seen general, increase thermal resistance through a reduction in radiative heat loss, and *Papilio xuthus* and *Papilio maackii* have the best insulation properties.

4.6. Average Surface Radiosit

In Figure 16, At x = 0 m, the radiosity was in the range of 439 to 455 W/m^2 reflecting similar baseline thermal radiative performance. Nevertheless, upon increasing distance, different distinctions were observed between the bioinspired and traditional models. traditional model: The surface radiosity peaked quickly at x = 1.5 m to a value of 534.6 W/m^2, after which it began to decrease slowly. Radiosity steadily decreased beyond x = 3.5 m, to values near 468 W/m^2 at x = 6 m. This implies that there is a strong absorption at the beginning and difficulty to maintain constant thermal radiations at long distances. *Kaniska canace* model: This model exhibited the maximum radiosity 518.9 W/m^2 at x = 1.5 m, however thereafter the decrease was smoother than in the traditional case. At x = 6 m the value decreased to approximately 474.6 W/m^2 and it appears that despite being very efficient initially, its ability to retain radiative stability over long range. *Papilio xuthus* model: This model made marginally lower peak radiosity 514.5 W/m^2 at x = 1.5 m than *Kaniska canace*, however, had a smoother drop pattern. radiosity at x = 6 m was approximately 475.7 W/m^2 slightly greater than *Kaniska canace*. This implies better thermal stability over distances, which is explained by

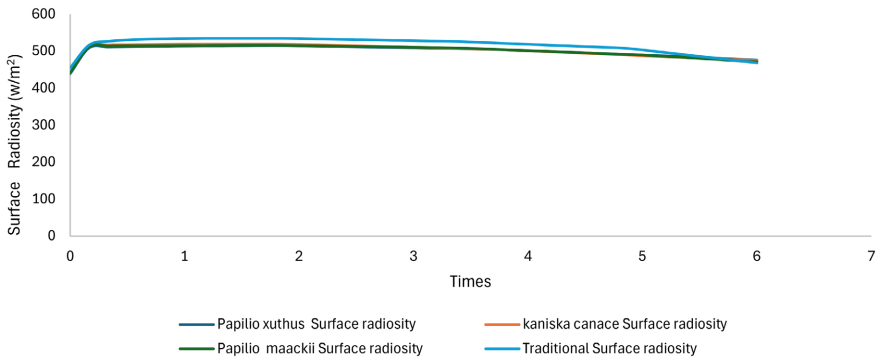

Figure 16. Surface radiosity-time curve chart of bionic model.

better light-trapping microstructures. *Papilio maackii* model: This model provided the most consistent radiosity profile with the maximum of 515.8 W/m^2 and comparatively high performance throughout the whole distance range. Radiosity even at $x = 6$ m was 470.7 W/m^2, with a slower rate of decrease than in the conventional model. This indicates that *Papilio maackii*'s surface morphology optimizes both absorption and redistribution of incident radiation.

5. Conclusion

This study demonstrated that the butterfly wing microstructures with ordered ridges and cavities which trap and reflect light can be effectively modeled into biomimetic thermal insulation applications. The bioinspired designs showed much lower temperature gradient, surface heat flux, and surface radiosity profile stability in comparison to conventional smooth surfaces, which is an indicator of better thermal resistance. Out of the three species studied, *Papilio xuthus* and *Papilio maackii* produced the best insulation performance with *Kaniska canace* scoring intermediate efficiency. However, every bioinspired design performed better than the conventional design. The results assert that natural thermoregulatory mechanisms of butterfly wings, such as low thermal conductivity, illustrate that the microstructures of butterfly wings could be implemented to thermal panels in order to increase insulation properties. This holds significant consequences to energy-efficient building envelopes in warm and moisture-rich regions like West Africa, where traditional building practices have a tendency to fail in creating thermal comfort. The proposed future research must focus on experimental modeling and verification of the simulated biomimetic models with additive manufacturing (3D printing) with polylactic acid (PLA). This will enable testing of the fact that the theoretical and simulated predictions are in line with the actual thermal performance in real climatic conditions. The experimental stage would also allow assessing the technical feasibility and scalability of such panels production to have practical applications in building activities. The current research however, failed to make a general comparison with the modern thermal insulation material in common use in West Africa as expanded polystyrene (EPS), polyurethane foam and polyethylene-based composite which somewhat limits the range of its economic evaluation. Another research must hence involve comparative benchmarking and lifecycle cost analysis in order to determine the level of competitiveness and sustainability of bioinspired insulation panels over these current market solutions in the local building setting.

Conflicts of Interest

The authors declare no conflicts of interest regarding the publication of this paper.

References

[1] Ali, A., Issa, A. and Elshaer, A. (2024) A Comprehensive Review and Recent Trends in Thermal Insulation Materials for Energy Conservation in Buildings. *Sustainability*,

16, Article 8782. https://doi.org/10.3390/su16208782

[2] Klemczak, B., Kucharczyk-Brus, B., Sulimowska, A. and Radziewicz-Winnicki, R. (2024) Historical Evolution and Current Developments in Building Thermal Insulation Materials—A Review. *Energies*, **17**, Article 5535. https://doi.org/10.3390/en17225535

[3] Kajjoba, D., Wesonga, R., Lwanyaga, J.D., Kasedde, H., Olupot, P.W. and Kirabira, J.B. (2025) Assessment of Thermal Comfort and Its Potential for Energy Efficiency in Low-Income Tropical Buildings: A Review. *Sustainable Energy Research*, **12**, Article No. 25. https://doi.org/10.1186/s40807-025-00169-9

[4] Chen, X., Vand, B. and Baldi, S. (2024) Challenges and Strategies for Achieving High Energy Efficiency in Building Districts. *Buildings*, **14**, Article 1839. https://doi.org/10.3390/buildings14061839

[5] Lazaro, S.A.M. and Li, X. (2025) Evaluating the Feasibility and Challenges of Using Passive Solar Systems for Achieving Thermal Comfort in African Countries: A Review. *International Journal of Building Pathology and Adaptation*. https://doi.org/10.1108/ijbpa-05-2024-0109

[6] Leo Samuel, D.G., Dharmasastha, K., Shiva Nagendra, S.M. and Maiya, M.P. (2017) Thermal Comfort in Traditional Buildings Composed of Local and Modern Construction Materials. *International Journal of Sustainable Built Environment*, **6**, 463-475. https://doi.org/10.1016/j.ijsbe.2017.08.001

[7] Jalali, S., Badarnah, L. and Nicoletti, E. (2025) Biomimetic Adaptive Solar Building Envelopes: Trends, Challenges, and Opportunities for Sustainable Applications. *Renewable and Sustainable Energy Reviews*, **215**, Article ID: 115586. https://doi.org/10.1016/j.rser.2025.115586

[8] Jessop, A., Pirih, P., Wang, L., Patel, N.H., Clode, P.L., Schröder-Turk, G.E., *et al.* (2024) Elucidating Nanostructural Organization and Photonic Properties of Butterfly Wing Scales Using Hyperspectral Microscopy. *Journal of the Royal Society Interface*, **21**, Article ID: 20240185. https://doi.org/10.1098/rsif.2024.0185

[9] Xu, N., Wang, J., Cui, Y., Ren, S., Deng, J., Gou, Q., *et al.* (2024) Butterfly Wing-Inspired Microstructured Film with High Reflectivity for Efficient Passive Radiative Cooling. *Renewable Energy*, **229**, Article ID: 120732. https://doi.org/10.1016/j.renene.2024.120732

[10] Zhang, H., Ly, K.C.S., Liu, X., Chen, Z., Yan, M., Wu, Z., *et al.* (2020) Biologically Inspired Flexible Photonic Films for Efficient Passive Radiative Cooling. *Proceedings of the National Academy of Sciences of the United States of America*, **117**, 14657-14666. https://doi.org/10.1073/pnas.2001802117

[11] Liu, G., Chen, H., Yin, Y., Chen, Y. and Liu, Y. (2023) Bionic Research of Photothermal Conversion Performance Based on Butterfly Wings. *Entomological Research*, **53**, 390-403. https://doi.org/10.1111/1748-5967.12673

[12] Tien, C.L. and Lienhard, J.H. (1979) Statistical and Physical Methods in Heat Transfer. Prentice-Hall.

[13] Bejan, A. (2000) Shape and Structure, from Engineering to Nature. Cambridge University Press.

[14] Ramakrishma Doodi, G.B. (2023) Experimental and Analytical Investigation of Bio-Inspired Lattice Structure under Compressive Loading. *Engineering Research Express*, **5**, Article ID: 035035.

[15] Mitchell, J.W. and Braun, J.L. (2022) Energy plus Engineering Reference: The Reference to Energy plus Calculations. U.S. Department of Energy, 105 p.

https://energyplus.net/assets/nrel_custom/pdfs/pdfs_v24.2.0/EngineeringReference.pdf

[16] WeatherSpark (2025) Historical Weather in January 2025 in Abidjan, Côte d'Ivoire—Hourly Wind Speed. https://weatherspark.com/h/m/35113/2025/1/Historical-Weather-in-January-2025-in-Abidjan-Côte-d'Ivoire

[17] Kone, D., Tuo, S., Coulibaly, K.A., Olivier Gore, B.T., Dje, K.B., Traore, M., *et al.* (2024) Assessment of Wind Potential Energy of Four Major Cities in Cote d'Ivoire Using Satellite Data from 2015 to 2022. *Journal of King Saud University—Science*, **36**, Article ID: 103579. https://doi.org/10.1016/j.jksus.2024.103579

[18] Weather Spark (2025) Average Weather in Abidjan, Côte d'Ivoire, Year-Round. Weather Spark. https://weatherspark.com/y/35113/Average-Weather-in-Abidjan-C%C3%B4te-d%E2%80%99Ivoire-Year-Round

[19] Auras, R., Harte, B. and Selke, S. (2010) Polylactic Acid: Synthesis, Properties, and Applications. In: Moo-Young, M., Ed., *Comprehensive Biotechnology* (2*nd Edition*), Elsevier, 434.

[20] Helgi Analytics (2022) Cassava Production Fell 0.037% to 6,300 kt in Ivory Coast in 2022. Helgi Library. https://www.helgilibrary.com/charts/cassava-production-fell-0037-to-6300-kt-in-ivory-coast-in-2022/

[21] 2SCALE (2023) Strengthening the Poultry Sector through Improved Maize Production in Côte d'Ivoire. 2SCALE Initiative. https://www.2scale.org/en/updates/strengthening-the-poultry-sector-through-improved-maize-production-in-cote-d-ivoire-en

[22] Zhang, X., *et al.* (2020) Thermal and Mechanical Properties of Annealed PLA for Engineering Applications. *Polymers*, **12**, Article 2091.

[23] Kouadio, J., Yao, A. and N'Guessan, K. (2024) Assessment of Urban Heat Island Intensity and Its Relation to Land Surface Temperature in Abidjan, Côte d'Ivoire. *Atmosphere*, **15**, Article No. 758.

[24] Çelik, I.B., Ghia, U., Roache, P.J. and Freitas, C.J. (2008) Procedure for Estimation and Reporting of Uncertainty Due to Discretization in CFD Applications. *Journal of Fluids Engineering*, **130**, Article ID: 078001.